Ceramics International 42 (2016) 13248–13255

Contents lists available at ScienceDirect

Ceramics International

journal homepage: www.elsevier.com/locate/ceramint

Highly dense and textured superconducting $(Bi,Pb)_2Sr_2Ca_2Cu_3O_{10+\delta}$ ceramic samples processed by spark-plasma texturing

L. Pérez-Acosta [a], E. Govea-Alcaide [b], J.G. Noudem [c], I.F. Machado [d], S.H. Masunaga [e], R.F. Jardim [e,*]

[a] Departamento de Física, Facultad de Electromecánica, Universidad de Camagüey, Circunvalación Norte Km 5 1/2s/n, Camagüey, Cuba
[b] Departamento de Física-Matemática, Facultad de Ciencias Informáticas, Naturales y Exactas, Universidad de Granma, Apdo. 21, P. O. Box 85100, Bayamo, Cuba
[c] CRISMAT/LUSAC Laboratory, CNRS UMR 6508 ENSICAEN/CNRS and Université de Caen Basse-Normandie, 6 Bd Maréchal Juin, F-14050 Caen Cedex 04, France
[d] Departamento de Engenharia Mecatrônica e Sistemas Mecânicos, Escola Politécnica, Universidade de São Paulo, 05508-900, São Paulo, SP, Brazil
[e] Instituto de Física, Universidade de São Paulo, Rua do Matão, 1371, 05508-090, São Paulo, SP, Brazil

ARTICLE INFO

Article history:
Received 8 April 2016
Received in revised form
15 May 2016
Accepted 19 May 2016
Available online 21 May 2016

Keywords:
Cuprates superconductors
Texture
Spark-plasma
Anisotropy

ABSTRACT

Consolidated powders of the superconducting cuprate $Bi_{1.65}Pb_{0.35}Sr_2Ca_2Cu_3O_{10+\delta}$ (Bi-2223) by the spark-plasma texturing (SPT), spark-plasma sintering (SPS), and the traditional solid-state reaction method were investigated by several techniques and their features compared. The results show that SPT samples exhibit a higher degree of texture, as inferred by a Lotgering factor of ~0.73 along the [00*l*] direction and a relative density of 96% of the theoretical value. From magnetic hysteresis loops *M* vs. *H* at 5 K, the intragranular critical current densities along two applied magnetic field orientations, J_{c0}^{c} and J_{c0}^{ab}, relative to the compacting pressure direction, were determined. The anisotropy factor, $\gamma_J = J_{c0}^{ab}/J_{c0}^{c}$, yielded an estimate of ~2 in the SPS sample and ~19 for samples obtained via the SPT method. In the latter samples, J_{c0}^{c} at 5 K is close to 1.3×10^8 A/cm^2, a value higher than others found for the same compound. The temperature dependence of the electrical resistivity, $\rho(T)$, analyzed within the framework of a current conduction model for granular superconductors, supports the higher degree of texture of SPT samples and indicates changes in the oxygen content when samples are subjected to a post-annealing heat treatment. All the results reveal the promising capabilities of the SPT method for improving volume density, texture, and grain boundary connectivity of superconducting Bi-2223 materials.

1. Introduction

The layered crystal structure of copper-oxide superconductors results in highly anisotropic properties. In particular, the anisotropy in transport properties of these materials is one of the most important factors in limiting their practical applications [1]. Other important barrier for the current transport in these granular materials is related to a broad distribution of grain boundaries misorientation [2]. Such a broad distribution promotes the existence of different scales of superconducting currents, also referred to as electromagnetic granularity [2]. Previous studies revealed the existence of three different superconducting levels in polycrystalline specimens: (i) the superconducting grains; (ii) the superconducting clusters; and (iii) the weak-links. Indeed, several experimental results support that the transport properties in the last two levels strongly depend on the texture degree of the samples and grain connectivity [3].

Within this scenario, development of highly-textured cooper-oxide superconducting ceramics is of paramount importance for producing materials with high values of critical current densities, J_c. In fact, several different procedures have been employed to enhance the degree of texture in high-T_c superconductors [4]. Generally, such procedures require a complex deformation and reaction processes under extreme conditions, e.g., higher mechanical deformations and temperatures, larger sintering times, etc. In the last decade, the well known spark-plasma sintering (SPS) method has proven to be a very attractive alternative for improving density in a variety of ceramic materials including ferroelectrics, superconducting oxides, etc [5,6]. By using the SPS method, ceramic materials with more than 98% of theoretical density may be obtained [7]. Such a very high density is commonly achieved by using higher heating rates, moderate compacting pressures, and lower sintering temperatures and sintering times. Moreover, we have consolidated, by using the SPS technique, pre-

* Corresponding author.
E-mail address: rjardim@if.usp.br (R.F. Jardim).

http://dx.doi.org/10.1016/j.ceramint.2016.05.122
0272-8842/

reacted powders of $Bi_{1.65}Pb_{0.35}Sr_2Ca_2Cu_3O_{10+\delta}$ (Bi-2223) and have obtained pellets with ~85% of the theoretical density value even by using mild conditions as an uniaxial compaction pressure of 50 MPa, low temperatures (~100 °C below the usual ones), and for just 5 min [8]. However, the application of the SPS method may result in pellets with a very low degree of texture, a moderate density, and heterogeneous microstructures, the latter mostly from the center to the outer region of cylindrical-shaped specimens [9].

On the other hand, it is well known that the electrical transport properties in these anisotropic layered materials are strongly influenced by the grain alignment along the $a-b$ planes of the unit cell [10]. Taking the Bi-2223 material as an example, ceramic samples subjected to different uniaxial compacting pressures before the last heat treatment were found to exhibit anisotropic superconducting properties [11]. The authors also found that in a range of uniaxial compacting pressures, roughly from 90 to 600 MPa, Bi-2223 samples showed a high degree of texture, with their grains well oriented along the *c*-axis, i. e., parallel to the uniaxial compacting direction. This partial orientation of the grains resulted in a higher volume density of the material and a better connectivity between grains, a feature also observed elsewhere [12].

We describe here our efforts to obtain highly textured and dense $Bi_{1.65}Pb_{0.35}Sr_2Ca_2Cu_3O_{10+\delta}$ ceramic samples by using, besides the SPS process, an alternative method to the SPS technique: the spark-plasma texturing (SPT) method [9]. Phase composition, texture, and morphology of the materials have been investigated by using X-ray diffraction (XRD) and scanning electron microscopy (SEM). The samples were also characterized by magnetic field dependence of the magnetization $M(H)$ and temperature dependence of the electrical resistivity $\rho(T)$. The main contribution of the paper is to offer an alternative procedure for obtaining, under relatively mild sintering conditions, dense Bi-2223 ceramic samples with a very high degree of texture, and high superconducting critical current densities suitable for practical applications.

2. Experimental procedure

Powders of $Bi_{1.65}Pb_{0.35}Sr_2Ca_2Cu_3O_{10+\delta}$ (Bi-2223) were prepared by using the conventional solid-state reaction method, as described in details in the Ref. [8]. After this step, three portions of the pre-reacted powders of Bi-2223 were separated for the final consolidation under different methods: (i) the conventional sintering [13]; (ii) the spark-plasma sintering (SPS) [8]; and (iii) the spark-plasma texturing (SPT) [9].

In the conventional sintering, a portion of the pre-reacted powders were uniaxially pressed at 50 MPa in a mold of 20 mm in diameter. The resulting pellet was subjected to a heat treatment in a Lindberg/Blue tubular furnace at 843 °C, in air for 2400 min. For comparison reasons, this sample (REF) will thereafter be referred to as Reference sample.

For the SPS consolidation, another portion of Bi-2223 powders were placed inside a cylindrical graphite die with dimensions of 50 mm (outer diameter) and 20 mm (inner diameter) and between two graphite plungers of ~40 mm in height. The die was then placed inside the chamber of the SPS apparatus and sintering was performed under vacuum (from 10 to ~30 Pa) and the maximum uniaxial compacting pressure was 50 MPa. A detailed description of the preparation method employed was reported elsewhere [8]. Here, the SPS consolidation was performed in the Spark-Plasma Sintering System (SPSS) 1050 Dr Sinter® apparatus and under the following sintering conditions: consolidation temperature $T_D=750$ °C, heating rate $HR=145$ °C/min, and dwell time, $t_D=5$ min The samples obtained by this method will be referred to as SP.

In the SPT consolidation, the pre-reacted Bi-2223 powders were first shaped into pellets with a diameter of 13 mm by applying an uniaxial compacting pressure of 30 MPa. The shaped pellets were then pre-sintered in a Lindberg/Blue tubular furnace at 700 °C, in air for 120 min After this step, the pellets were easily accommodated at the center of a graphite die of a larger diameter of ~20 mm. Under this circumstance, there is a difference between the diameter of the pellet and the inner diameter of the graphite of 7 mm. As reported by Noudem et al. [9], the above feature avoids the direct contact between the outer surface of the pellet and the inner wall of the die. Consequently, the negative effect of the graphite-die wall is minimized, allowing the free deformation of the pellet. It is believed that this process results in an improved material with enhanced texture and low degree of defects such as voids and microcracks [9]. The final processing of the SPT pellets were carried out using the SPSS apparatus FCT System GmbH, HP D25, Rauenstein, Germany. The consolidation process was performed under vacuum (from 10 to ~30 Pa) and the maximum uniaxial compacting pressure was 50 MPa. The following sintering conditions were used: consolidation temperature, $T_D=750$ °C, heating rate, $HR=100$ °C/min, and dwell time, $t_D=15$ min Samples obtained by the SPT method will be referred to as ST.

As mentioned above, both SPS and SPT processes are conducted under vacuum and result in oxygen-deficient materials. It has been argued that such a deficiency is more pronounced close to the surface of the grains and grain boundaries [8,23]. In order to restore the optimum oxygen content of the materials, small cubes of both samples, SP and ST, were then subjected to an additional post-annealing heat treatment (PAHT). Such a heat treatment was performed in a Lindberg/Blue tubular furnace at 750 °C (heating and cooling rates of 5 °C/min) in air for 5 min, similarly as reported elsewhere [8]. These samples will be hereafter referred to as SP5 and ST5, respectively.

The phase identification was evaluated, in both powder and bulk samples, from X-ray diffraction patterns obtained in a Bruker-AXS D8 Advance diffractometer. These measurements were performed at room temperature using CuKα radiation in the $3° \le 2\theta \le 80°$ range with a 0.05° (2θ) step size, and 3 s counting time. The microstructure of the samples was investigated at room temperature using a high resolution Carl Zeiss (Supra 55, Oberkochen, Germany) Scanning Electron Microscope (SEM). SEM micrographs of faces broken parallel and perpendicular to the compacting pressure axis clearly show the morphology of the samples. Finally, the volume density, ρ_v, of all pellets was determined by using the Archimedes method.

All magnetization measurements were performed in pellets and powder samples by using a Physical Property Measurement System (PPMS) from Quantum Design. The magnetization as a function of the applied magnetic field, $M(H)$, was measured in the range of $-90 \le H \le 90$ kOe, for $T=5$ K. The samples were cooled down to 5 K under zero applied magnetic field. Once the temperature was stabilized, the magnetic field was applied along different orientations of the sample relative to the compacting pressure direction, i.e., $H \parallel ab$ and $H \parallel c$ refer to applied magnetic fields perpendicular and parallel to the compacting pressure direction, respectively. Also, the measurements were performed in small cube samples avoiding different corrections along the faces due to the demagnetizing factor.

The electrical resistivity as a function of temperature, $\rho(T)$, was measured by using the standard four-probe technique in slabs with typical dimensions of $d=0.5$ mm (thickness), $w=2$ mm (width), and $l=10$ mm (length). In these measurements, performed in the PPMS apparatus, Au electrical leads were attached to Ag film contact pads on samples using Ag epoxy. After cooling the

sample in zero applied magnetic field, an excitation current of 1 mA ($J = 10^{-2}$ A/cm^2) was applied always perpendicular to the compacting direction. The voltage across the sample and the temperature were collected as the temperature was raised slowly from 50 to 300 K.

3. Results and discussion

Fig. 1 displays the X-ray diffraction patterns taken on the surface of the samples SP5, ST5, REF, and in powders of the sample ST5, that was reground after the consolidation process. The analysis of the patterns reveals that all indexed reflections related to the high-T_c Bi-2223 have been observed, as displayed in panel (a) of Fig. 1. The peaks of the Bi-2223 phase were then indexed with respect to an orthorhombic crystal structure, space group A2aa, lattice parameters $a = 5.410$ Å, $b = 5.413$ Å, and $c = 37.152$ Å, in excellent agreement with those reported for the same compound elsewhere [14]. We have also detected an unknown reflection near $2\theta = 31.4°$, not associated with the Bi-2223 phase, in the X-ray diagram of sample ST5. Close to this angular position is located the reflection [117] belonging to the Bi-2212, as reported elsewhere [15]. However, the most intense reflection of the Bi-2212 phase, [115] and commonly observed at $2\theta = 27.4°$, is completely absent in our X-ray diagrams. On the other hand, SEM and energy dispersive X-ray spectroscopy (EDS) results obtained in Bi-2223 samples synthesized by the SPS technique were consistent with the presence of an extra phase in these materials [16]. Such an extra phase was identified as an infinite layer compound with general formula $Ca_{1-x}Sr_xCuO_2$ [17]. The kinetic formation of this compound, as a result of the SPT sintering of Bi-2223 pellets, is still object of study.

From the X-ray diffraction patterns, we have also estimated the Lotgering factor along the [00l] direction, $L_{(00l)}$ [18], and selected values are listed in Table 1. We have found that $L_{00l} = 0.32$ in sample SP5 and reaches a very high value of ~0.73 in both ST samples (ST and ST5). We have also observed that $L_{(00l)}$ in ST samples is over two times higher than that one calculated for the SP sample, and ~7 times higher than the reference sample, where $L_{(00l)}$ is only 0.11. These results indicate a very high degree of texture in samples consolidated by the SPT method.

The very high degree of texture of the ST samples may also be verified visually by inspecting the relative intensity of some Bragg reflections of the type (h00) and (00l) (see dashed boxes in Fig. 1). We first note here that the behavior of these Bragg peaks obeys a similar trend in the powder (Fig. 1(a)), the SP5 (Fig. 1(b)), and REF (Fig. 1(d)) samples: the relative intensity of the reflection (200) is always greater than (0014). On the other hand, however, the relative intensity of these peaks in the ST5 sample is quite different: its most intense reflections are those along the [00l] direction, further indicating a very high degree of texture along the c-axis of the material.

The above results may have their counterpart in the microstructure of the samples studied. This can be inferred from the surface and fracture micrographs of samples SP5 and ST5, displayed in Fig. 2(a)–(b) and (c)–(d), respectively. The high magnification micrographs show samples with similar granular morphology and grain size besides the occurrence of grains with a platelet-like shape. The average grain size in both samples was estimated to be $L_a = L_b \approx 6$ μm long, and as thick as $L_c \sim 0.16$ μm. In addition to that, a much better alignment of the platelet-like grains along their minor lengths (c-axis), or more appropriately a high degree of texture, is clearly seen in the ST5 sample. The combined features observed in the SEM micrographs are in line with those extracted from X-ray diffraction data, i.e., the Lotgering factors along the direction [00l].

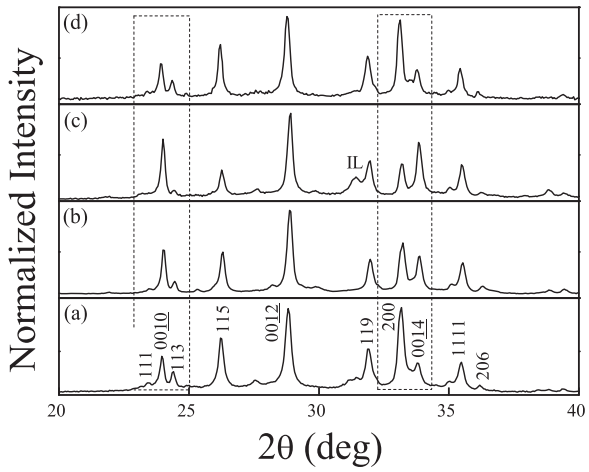

Fig. 1. The X-ray diffraction patterns of the powdered ST5 sample (a), and of bulk samples SP5 (b), ST5 (c) and REF (d). The X-ray data of the pellets were taken on the surface perpendicular to the compacting pressure direction. The reflections belonging to the Bi-2223 phase are marked by Miller indexes in (a). Selected regions of the diagrams, marked as dashed boxes, are discussed in the text.

Table 1.
Some parameters of the samples studied in this work: ρ_v is the volume density, $L_{(00l)}$ is the Lotgering factor along the direction [00l], M_r^{ab} and M_r^c are the remanent magnetization in two directions: $H \parallel c$ and $H \parallel ab$, respectively. γ_M is the ratio M_r^{ab}/M_r^c at 5 K, J_{c0}^{ab} and J_{c0}^c are the extrapolated ($H = 0$) intragranular critical current densities along the directions $H \parallel c$ and $H \parallel ab$ measured at 5 K, respectively, and γ_J is the ratio J_{c0}^{ab}/J_{c0}^c.

Sample	ρ_v $\left(\frac{g}{cm^3}\right)$	L_{00l}	M_r^{ab} $\left(\frac{emu}{cm^3}\right)$	M_r^c $\left(\frac{emu}{cm^3}\right)$	γ_M	J_{c0}^{ab} $\left(10^8 \frac{A}{cm^2}\right)$	J_{c0}^c $\left(10^8 \frac{A}{cm^2}\right)$	γ_J
ST	6.3	0.73	27.3	24.8	1.1	0.91	0.08	12
ST5	6.3	0.73	38.5	25.7	1.5	1.27	0.07	19
SP5	5.7	0.32	24.1	16.2	1.5	0.26	0.13	2
REF	3.2	0.11	21.1	20.6	1.0	0.21	0.13	1.6

The SEM micrographs also indicate that samples SP5 and ST5 have a very high density. Such a statement is confirmed by the values of the volume density, ρ_v, of all samples studied and displayed in Table 1. As expected, sample SP5 was found to have a density of 5.7 g/cm^3, ~86% of the theoretical value for Bi-2223 (6.6 g/cm^3) [19]. Based on a previous report [8], we speculate that ρ_v is limited to 5.7 g/cm^3 when the SPS method is used to consolidate Bi-2223 powders. This limitation would be related to the mechanical properties of the graphite die used in these experiments, which is mainly restricted to applied compacting pressures in the range 80–100 MPa. However, samples ST and ST5 exhibit a higher value of density, close to 6.3 g/cm^3, i.e., ~96% of theoretical density at 50 MPa. The above results assure the capabilities of the SPT process to obtain highly dense and textured superconducting samples, as reported elsewhere in other materials [9]. On the other hand, the reference sample has $\rho_v = 3.2$ g/cm^3, a value that hardly reaches 50% of the theoretical value.

In order to evaluate the texture of the samples and the effectiveness of the SPT method against the conventional SPS, $M(H)$ measurements were performed in selected samples for different orientations of H with respect to the compacting pressure. Fig. 3 (a) displays typical hysteresis loops $M(H)$ curves measured in sample ST5 at 5 K. The most important results here may be summarized as follows: (i) the behavior of both curves strongly depends on the magnitude of H; (ii) the $M(H)$ curves exhibit a definite anisotropy when different orientations of H are considered;

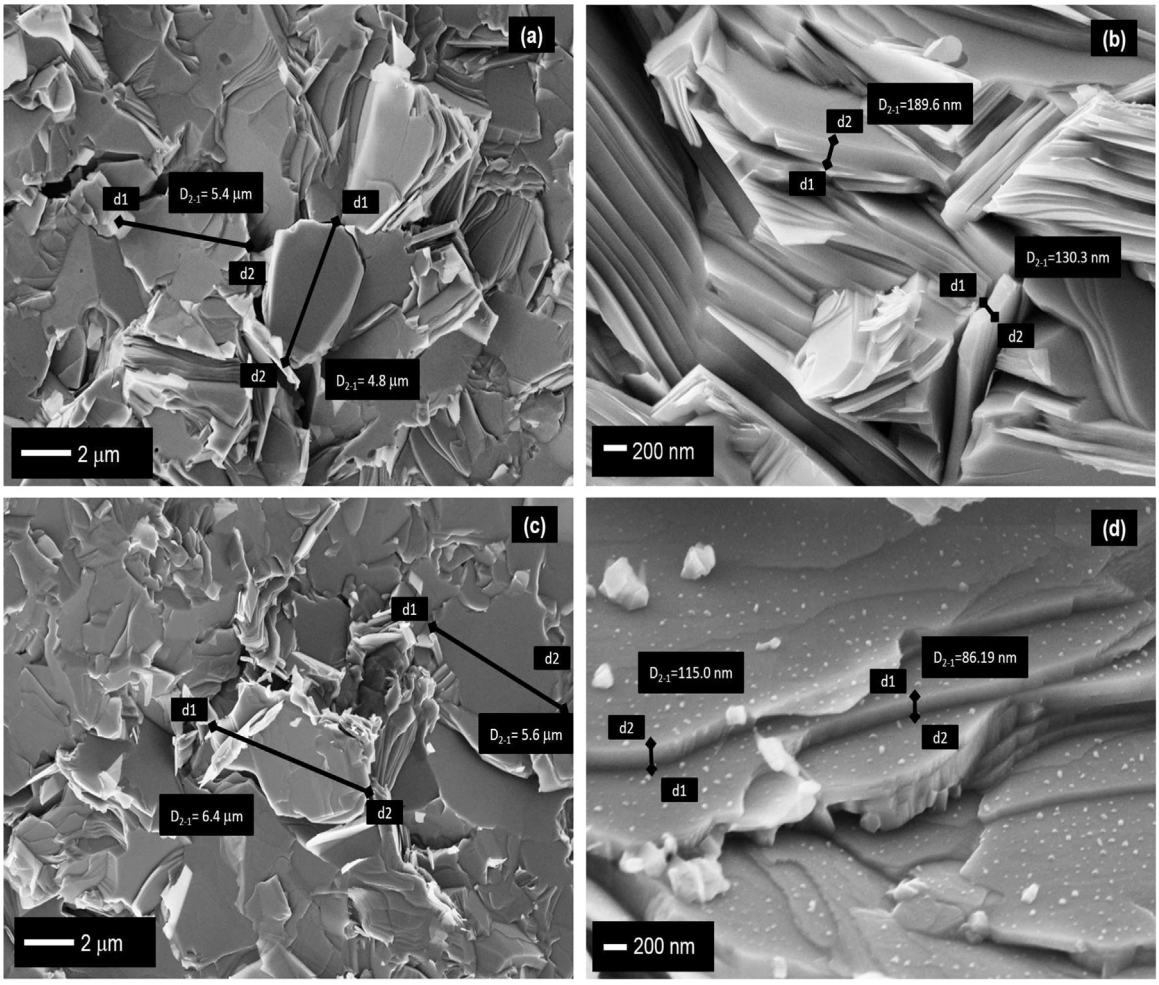

Fig. 2. Scanning electron micrographs of surface and fracture surfaces of samples SP5 (a), (b) and ST5 (c), (b).

and (iii) the magnetization measured parallel to the compacting pressure direction, $H \parallel c$, is always higher than those measured along $H \parallel ab$. These results are particularly mirrored in the behavior of the remanent magnetization, $M_r = M(0)$, as listed in Table 1. We mention that M_r is closely related to the magnetic flux trapped within samples as well as their pinning strength [20,21]. According to values of M_r along $H \parallel ab$ (M_r^c) and $H \parallel c$ (M_r^{ab}), the magnetic flux trapped by samples ST and ST5 is greater than that of sample SP5. However, the ratio $\gamma_M = M_r^{ab}/M_r^c$ (see Table 1) is ~1.5 when samples ST5 and SP5 are considered and only 1.1 for sample ST. These values of γ_M are similar to those reported for the same compound [22] and the difference in γ_M between samples ST and ST5 may be understood by considering the post-annealing heat treatment (PAHT) through which the ST5 sample has been subjected.

Similarly to the SPS method, the consolidation process in the SPT takes place under vacuum, resulting in oxygen-deficient samples, or more appropriately, grains with core-shell morphology comprising of: (i) a core of stoichiometric Bi-2223 phase; and (ii) an oxygen-deficient shell, as discussed elsewhere [8]. The PAHT is then responsible for the re-oxygenation of grains and grain boundaries of the dense material, the latter being strong altered and then comprised of a large number of conduction current paths in oxygenated materials [23]. The observed different values of $\gamma_M = M_r^{ab}/M_r^c$ between samples ST and ST5 may be connected to the re-oxygenation process promoted by the PAHT: it is responsible for the decrease in the width of the oxygen-deficient shell of the grains. Such a decrease is expected to alter the superconducting volume fraction of the grains and the number and nature of pinning centers within the shell, i.e., very close to the grain boundaries [23]. In order to put this point in perspective, let us assume that the remanent magnetization stems mostly from the intragranular screening currents. In this case, $M_r = f_g M_g$, where f_g is the effective volume fraction of the grain cores and M_g is the intrinsic intragranular magnetization [24]. As the phase composition and the texture degree of samples ST5 and ST are similar (see Fig. 1 and Table 1), M_g is assumed to be the same for both samples. Within this context, the ratio M_r^{ab} for samples ST5 and ST is $f_{ab}^g = f_g^{ST5}/f_g^{ST} \sim 1.41$, indicating an increase of the superconducting volume fraction of the grains after the PAHT, i.e., a decrease in the width of the oxygen-deficient shell of the grains. It is important to notice that the estimate of f_g^c, by using values of M_r^c, yielded a value of ~1.04, further supporting the changes provoked by the PATH. The difference in the estimated values of f_g^{ab} and f_g^c also suggests that the oxygen-deficient shell is not homogeneously distributed over the entire surface of the grains. As schematically represented in the inset of Fig. 3(a), the oxygen-deficient shell can be viewed as a hollow tube surrounding the surface of the grains.

From the experimental $M(H)$ curves we were also able to estimate the intragranular critical current density by using the expression [25]:

$$J_c = 20 \times (M^+ - M^-)(L_x(1 - L_x/3L_y))^{-1}, \quad (1)$$

where M^- and M^+, in emu/cm^3, are the magnetizations associated with the decreasing and increasing branches of the $M(H)$

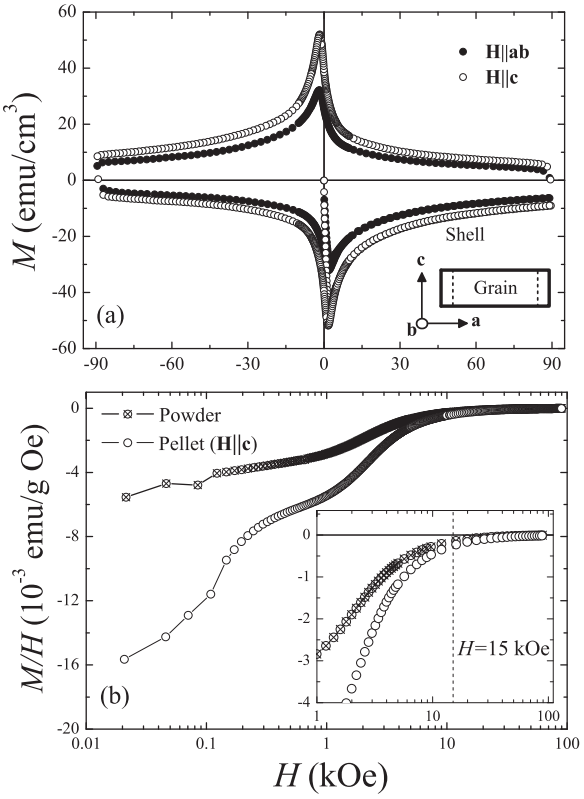

Fig. 3. (a) Hysteresis loops of M(H) at 5 K for different H orientations measured in the ST5 sample. (b) Magnetic field dependence of the dc magnetic susceptibility measured in a powder and pellet of the sample ST5 (see text for further details). Also, the inset shows in this figure an expanded view in the magnetic field range between 1 and 100 kOe.

data, respectively. Also, L_x and L_y ($L_y \geq L_x$), given in cm, are the average dimensions of the rectangular cross section of the grains perpendicular to H [25]. We mention here that the values of L_x and L_y in Eq. (1) refer to the physical dimensions of the physical grains instead of the macroscopic dimensions of the pellet as a whole. In line with this statement, Fig. 3(b) shows the magnetic field dependence of M, at 5 K, conducted in pellets and powders from sample ST5. This figure was constructed from the $M(H)$ data measured along $H \parallel c$ (see Fig. 3(a)). As observed, both $M(H)$ curves have different qualitative and quantitative behaviors up to $H \sim 10$ kOe (see the inset of Fig. 3(b)). In the powder sample, the almost magnetic field independent behavior of $M(H)$ up to 1 kOe is related to the magnetic flux shielding from isolated grains [23,26]. On the contrary, however, the magnetic responses of the pellet sample are comprised of two contributions stemming from the intragranular and the intergranular shielding currents. The former is expected to be very similar in pellet and powder samples. Thus, the difference observed between the two $M(H)$ curves of Fig. 3(b), for $H \leq 10$ kOe, is due to the influence of the intergranular shielding capability of the material. Nevertheless, as observed in the inset of Fig. 3(b) for $H \geq 10$ kOe, both $M(H)$ curves merge with each other, revealing quite a similar behavior. This is a remarkable result and indicates that:

- the pellet samples behave as isolated grains for applied magnetic fields higher than 10 kOe, further supporting the use of L_x and L_y of the grains in Eq. (1) for estimating the superconducting critical current of the samples;
- $\Delta M = M^+ - M^-$, in Eq. (1), is calculated from the $M(H)$ data for applied magnetic fields higher than 10 kOe;
- values of J_c obtained from Eq. (1), $H \geq 10$ kOe, are associated with the intragranular critical current of the specimen.

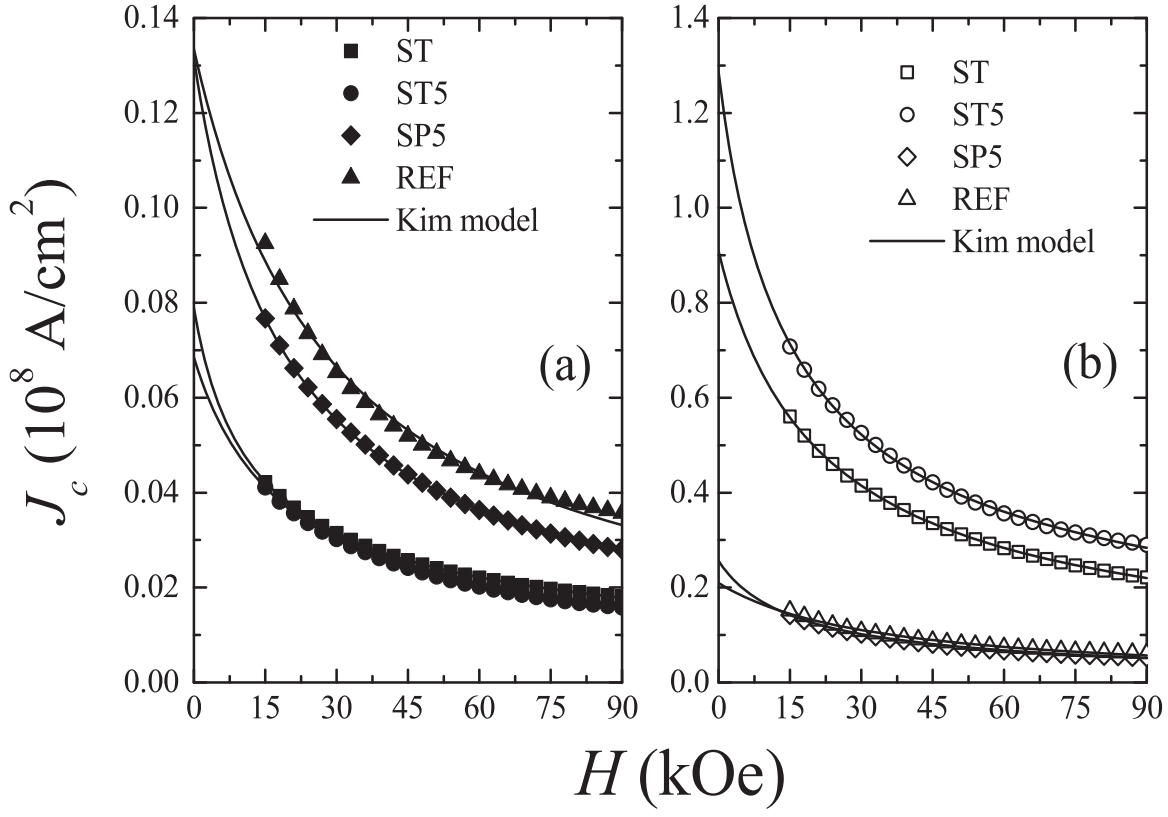

Fig. 4. Intragranular critical current densities $J_c(H)$ determined from M(H) data for all samples for $H \| ab$ (a) and $H \| c$ (b), respectively. Solid lines are theoretical fittings, as described in the text.

Fig. 4 displays the intragrain current density, $J_c(H)$, of samples ST, ST5, and SP5 subjected to applied magnetic fields along two different directions: $H \parallel ab$ (4(a)) and $H \parallel c$ (4(b)). In all cases, experimental values of $J_c(H)$ were calculated for $H \geq 15$ kOe. The results indicate that all curves exhibit a similar magnetic field dependence within the range 15–90 kOe. Also, the $J_c(H)$ curves were fitted to the expression $J_c(H) = J_{c0}(1 + (H/H_1))^{-1}$ [27], where J_{c0} is the critical current density at zero applied magnetic field, and H_1 is a material parameter. As displayed in Fig. 4(a) and (b), a very good agreement between experimental data and the Kim relation has been obtained. Values of J_{c0}, listed in Table 1, confirm the anisotropic behavior of $J_c(H)$ where the critical current density along $H \parallel c$ (J_{c0}^{ab}) is always higher than that from $H \parallel ab$ (J_{c0}^{c}). Moreover, the critical current density of sample ST5 along $H \parallel c$ is slightly higher than the observed in the ST sample and reaches, extrapolated to $H = 0$ Oe, 1.27×10^8 A/cm^2. This is a very high value of J_{c0} and it is tempting to compare it with others found in the literature.

Values of J_{c0} as high as $\sim 10^8$ A/cm^2 at 5 K in Bi-2223 are scarce in the literature. We first mention here an upper limit of $J_{c0} \sim 7.3 \times 10^9$ A/cm^2, measured at 10 K, in $Bi_2Sr_2Ca_2Cu_3O_{10+\delta}$ single crystals grown by the traveling solvent floating zone technique [28]. We also mention that $J_{c0} \sim 1.0 \times 10^7$ A/cm^2 (4.5 K) has been observed in multifilamentary Ag-sheathed Bi-2223 tapes, prepared by the powder-in-tube method [29]. On the other hand, our $J_{c0} \sim 1.3 \times 10^8$ A/cm^2 is similar to $J_{c0} \sim 1.0 \times 10^8$ A/cm^2 (4.2 K) found in Bi-2223 subjected to an uniaxial pressure of 500 MPa before the last heat treatment [22]. In addition to the high J_{c0} values of our SPT samples, the degree of texture/effectiveness of the spark-plasma texturing method must be considered. A measure of the degree of texture can be made by computing the anisotropy ratio $\gamma_J = J_{c0}^{ab}/J_{c0}^{c}$ (see Table 1). We have found that γ_J is ~12 and 19 in samples ST and ST5, respectively. This represents a ~6 to 9-fold increase in γ_J when compared to the sample SP5. Again, the observed difference in γ_J between samples ST and ST5 is ascribed to the post-annealing heat treatment PAHT, as mentioned above [8].

An alternative way to evaluate the effectiveness of the SPT method for producing dense Bi-2223 samples with a high degree of texture is considering the transport properties of the consolidated materials. Within this context, Fig. 5 displays the temperature dependence of the electrical resistivity, $\rho(T)$, of samples ST, ST5, SP5, and REF. We have first observed that all samples exhibit a metallic-like behavior of $\rho(T)$ and the transition to the superconducting state below $T_{on} \sim 118$ K (see Table 2). As T_{on} is related to the transition of isolated grains to the superconducting state, the comparable values of T_{on} encountered in all samples indicates that their grains, or more appropriately the core of the grains, have similar stoichiometry, a result in line with the X-ray diffraction analysis. On the other hand, the approaching to the zero resistance state occurs at quite different temperatures T_{off} along the series, as displayed in the inset of Fig. 5(b). T_{off}, that mainly depends on the intergranular features of a granular superconductor, was found to attain very low values in the oxygen-deficient sample ST (90.5 K) and the reference sample REF (86.5 K). On the contrary, T_{off} assumes much higher values in samples SP5 (97.3 K) and ST5 (96.5 K), subjected to the post-annealing heat treatment (PAHT). At first glance, the REF sample, with the lowest value of T_{off}, has a very weak connectivity between grains due to its very low volume density (see Table 1). The other SPS and SPT samples, subjected or not to the post-annealing heat treatment PAHT, have a very high volume density and display higher values of T_{off}, suggesting a better intergrain connectivity. In addition to that, the normal-state electrical resistivity of sample ST, with $T_{off} \sim 90.5$ K, is ~30% lower than that of the SP5 (Fig. 5(a)), further indicating that there is an intricate balance among the contributions to the $\rho(T)$ behavior in this series, i. e., the volume density,

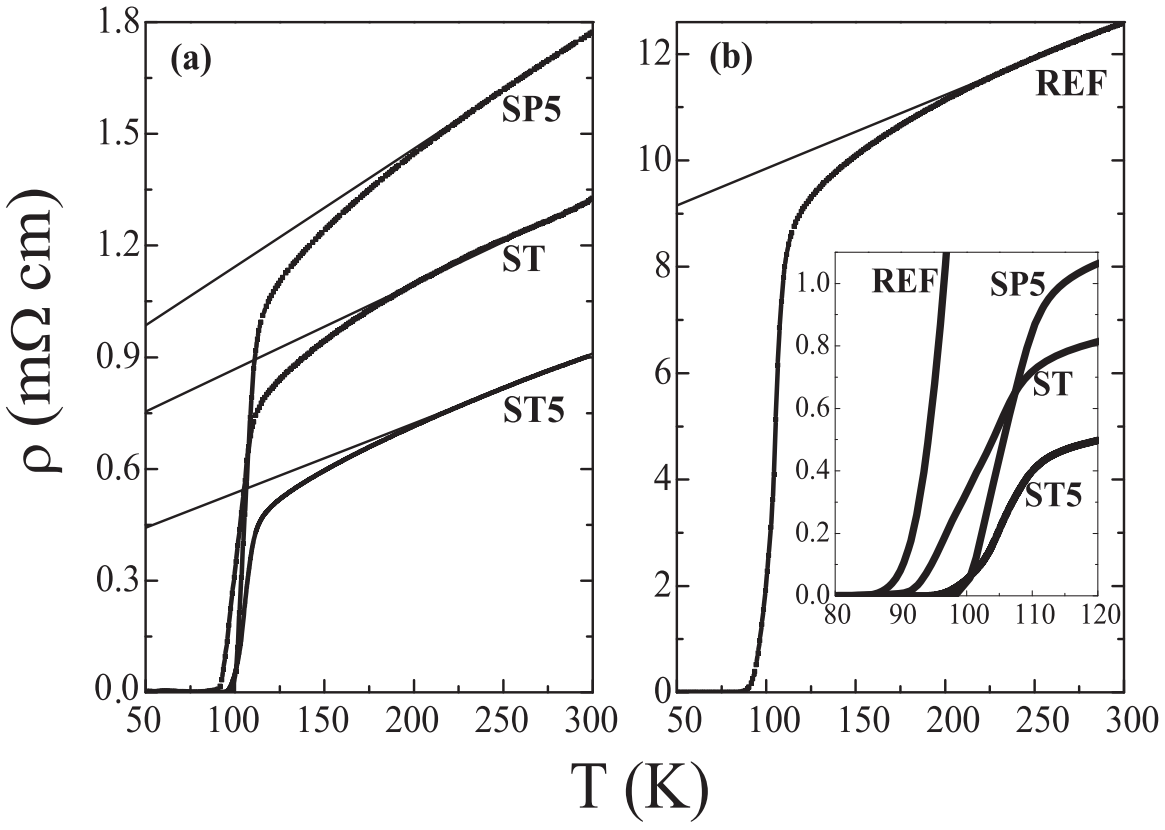

Fig. 5. Temperature dependence of the electrical resistivity of samples ST, ST5, SP5 (a), and the reference sample (b). The continuous lines are linear fits in the normal state region. The inset in (b) displays an expanded view of the superconducting transition region.

Table 2.
Parameters extracted from the $\rho(T)$ curves of all samples studied: the onset superconducting critical temperature, T_{on}; the offset temperature, T_{off}; the slope of the electrical resistivity data in the T-linear region, A; the residual electrical resistivity, $\rho(0)$; the normal-state percolative factor, α_n; and the average intergranular electrical resistivity, ρ_{wl}.

Sample	T_{on}(K)	T_{off}(K)	A(μΩ cm/K)	ρ (0) (mΩ cm)	α_n	ρ_{wl} (mΩ cm)
ST	117.6	90.5	2.14	0.67	0.85	0.57
ST5	117.6	96.5	1.93	0.33	0.95	0.31
SP5	118.3	97.3	3.26	0.80	0.56	0.45
REF	118.2	86.5	14.4	8.29	0.13	1.08

the degree of texture, and the oxygen content. In any event, the $\rho(T)$ data indicate that the microstructural features of the samples, along the post-annealing heat treatment PATH, have a definite influence on the transport properties of these materials, as discussed below.

In order to extract extra microstructural information regarding our samples from $\rho(T)$ data, the model first proposed by Díaz et al. was considered [10]. In such a model, based on the effective-medium theory, the normal-state $\rho(T)$ behavior of polycrystalline samples of high temperature superconductors is described as a sum of two contributions: (i) one related to the anisotropic and assumed single-crystal grains, weighted by the misalignment of adjacent grains along their *ab*-planes; and (ii) another one, stemming from microstructural defects such as voids, microcracks, insulating grain boundaries, etc. Within the context of the model, the $\rho(T)$ dependence is written as follows [10]:

$$\rho(T) = \frac{1}{\alpha_n}(\rho_{ab}(T) + \rho_{wl}), \tag{2}$$

where α_n, $0 < \alpha_n \leq 1$, given by

$$\alpha_n = f\alpha_{str}, \tag{3}$$

is referred to as the normal-state percolative factor that enhances the electrical resistivity due to both the misalignment of the grains f; $0 < f \leq 1$; and microstructural defects α_{str}; $0 < \alpha_{str} \leq 1$. The grains are believed to behave as single crystals and the first term in Eq. (2), $\rho_{ab}(T)$, is closely related to the average electrical resistivity of the anisotropic material along its *ab*-plane. The second term, ρ_{wl}, is the actual average intergranular component of the polycrystalline material, assumed to be temperature-independent. The $\rho_{ab}(T)$ contribution in our analysis has been assumed to be linearly temperature-dependent and zero-residual temperature intercept [30]. In addition to that, α_n and ρ_{wl} were obtained by utilizing the appropriate relationships [10]:

$$\alpha_n = \frac{A_{sc}}{A}, \tag{4}$$

and

$$\rho_{wl} = \alpha_n\rho(0), \tag{5}$$

where A is the slope of the $\rho(T)$ curve in the T-linear region, A_{sc}=1.84 μΩ cm/K for Bi-2223 single crystal [30], and $\rho(0)$ is the residual electrical resistivity at T=0. The parameters were obtained by fitting the $\rho(T)$ curves to the typical linear-dependence $\rho(T) = AT + \rho(0)$. The best fittings, by using the above T-linear dependence, were obtained by adjusting the parameters listed in Table 2. Values of α_n and ρ_{wl}, extracted by using Eqs. (4) and (5), are also displayed in Table 2.

The results listed in Table 2 indicate that ST samples, subjected to a process in which a high degree of texture is desired, display α_n values much higher than in samples SP5 and REF. In fact, the extracted α_n values from the $\rho(T)$ data of 0.85 and 0.95 for samples ST and ST5, respectively, are close to the unity and in excellent agreement with the very high Lotgering factors along the L_{00l} direction (see Table 1) and a highly textured material seen in the SEM image of Fig. 2(b). Returning to Eq. (3), we emphasize that α_n mainly depends on two contributions that enhances the electrical resistivity: (i) the misalignment of the grains f in a ceramic specimen; and (ii) microstructural defects α_{str}. The results displayed in Table 2 combined with the lower value of $\rho(T)$ observed in sample ST compared to sample SP5, as mentioned above, indicate that the degree of texture has a major contribution to change $\rho(T)$ in our granular and anisotropic materials. This is further confirmed when the contribution of microstructural defects to $\rho(T)$, ρ_{wl}, is considered. As listed in Table 2, ρ_{wl} ~0.57 of the ST sample is greater than ρ_{wl} ~0.45 of sample SP5 (see Table 2) but $\rho^{ST}(T) < \rho^{SP5}(T)$ in the normal state (see Fig. 5(a)).

Taking the above discussion into consideration, it is plausible to infer that $\rho(T)$ in REF sample is mainly dominated by the ρ_{wl}=1.08 mΩ cm term, i. e., microstructural defects like voids, microcracks, insulating grain boundaries etc. The microstructural defects, combined with a very low volume density ρ_v and a negligible degree of texture (α_n=0.13) result in a ~10 times large normal-state electrical resistivity of the REF sample (see Fig. 5(b)). This physical scenario is quite different when samples consolidated by the spark-plasma technique are considered. In these samples, where $\rho(T)$ is dominated by the very high degree of texture, the most important microstructural defect is certainly related to the oxygen-deficient shell of the grains, acting as insulating or low-conducting grain boundaries. Even though α_{str} may not be directly separated from α_n, changes caused by the post-annealing heat treatment PAHT on the $\rho(T)$ data can be evaluated. Let us consider the spark-plasma textured samples ST and ST5 with the same Lotgering factor (see Table 1) and similar values of α_n (see Table 2). Both samples are believed to have essentially the same value of f and by using Eq. (3), the ratio $\alpha_n^{ST5}/\alpha_n^{ST} = \alpha_{str}^{ST5}/\alpha_{str}^{ST} = 1.12$. Such an increase of 12% in α^{ST5} occurs at the expense of the decrease in the width of the oxygen-deficient shell of the grains [23]. This simple estimate indicates the importance of the post-annealing heat treatment PAHT in optimizing the normal-state and superconducting properties of dense and highly textured spark-plasma sintered samples of Bi-2223.

4. Conclusions

We have used the spark-plasma texturing SPT method to consolidate pre-reacted powders of Bi-2223 compounds and compared their physical properties with samples obtained by the conventional spark-plasma sintering process. The results of X-ray diffraction indicated that the SPT materials consist of the Bi-2223 phase and have Lotgering factors as high as 0.73. In these samples, the volume density reached 6.3 g/cm^3, a value close to 96% of the theoretical value and microstructures with a very high degree of texture. After a post-annealing heat treatment performed in air at 750 °C for only 5 min, the SPT samples exhibited an anisotropic intragranular critical current density and values as high as J_{c0}~1.3×10^8 A/cm^2 along $H \parallel c$ at T=5 K. We have also found that the normal and superconducting transport properties of our samples are strongly dependent on their oxygen content and the degree of texture. These results are of interest considering that samples were prepared under mild conditions, i.e., consolidated at 750 °C, under a low compacting pressure of 50 MPa, followed by a post-annealing heat treatment PAHT performed in air at 750 °C for a brief time interval of 5 min. We finally mention that dense polycrystalline samples with a very high degree of texture and J_{c0} at 5 K, as reported here in spark-plasma texturing samples, are

valuable for several practical applications.

Acknowledgements

The authors acknowledge financial support from Brazil's agencies FAPESP (Grant Nos. 2014/19245-6 and 2013/07296-2), CNPq (Grant Nos. 2014-6/168255, 2014/444712-3 and 2010/304112-0), and CAPES/MES (Grant Nos. 1470/2010 and 157/2012), and the Petrobras Company (Grant Nos. SAP 4600264279/ FUSP 1809 and SAP 4600220603/ FUSP 1551). We also thank Mr. J. Lecourt for his technical support.

References

[1] J. Halbritter, Extrinsic or intrinsic conduction incuprates – anisotropy, weak links, and strong links, Phys. Rev. B 48 (1993) 9735–9746.
[2] D. Larbalestier, A. Gurevich, D.M. Feldmann, A. Polyanskii, High-Tc superconducting materials for electric power applications, Nature 414 (2001) 368–377.
[3] H. Hilgenkamp, J. Mannhart, Grain boundaries in high-T_c superconductors, Rev. Mod. Phys. 74 (2002) 485–549.
[4] Z. Gao, K. Togano, A. Matsumoto, H. Kumakura, Achievement of practical level critical current densities in $Ba_{1-x}K_xFe_2As_2$/Ag tapes by conventional cold mechanical deformation, Sci. Rep. 4 (2014) 4065 (and references therein).
[5] R. Orrù, R. Licheri, A.M. Locci, A. Cincotti, G. Cao, Consolidation/synthesis of materials by electric current activated/assisted sintering, Mater. Sci. Eng. B 63 (2009) 127–287.
[6] J.E. Garay, Current-activated, pressure-assisted densification of materials, Annu. Rev. Mater. Res. 40 (2010) 445–468.
[7] K. Tyagi, B. Gahtori, S. Bathula, V. Toutam, S. Sharma, N.K. Singh, A. Dhar, Thermoelectric and mechanical properties of spark plasma sintered Cu_3SbSe_3 and Cu_3SbSe_4: promising thermoelectric materials, Appl. Phys. Lett. 105 (2014) 261902.
[8] E. Govea-Alcaide, I.F. Machado, M. Bertolete-Carneiro, P. Muné, R.F. Jardim, Consolidation of Bi-2223 superconducting powders by spark plasma, J. Appl. Phys. 112 (2012) 113906.
[9] J.G. Noudem, D. Kenfaui, D. Chateigner, M. Gomina, Toward the enhancement of thermoelectric properties of lamellar $Ca_3Co_4O_9$ by edge-free spark plasma texturing, Scr. Mater. 66 (2012) 258–260.
[10] A. Díaz, J. Maza, F. Vidal, Anisotropy and structural-defect contributions to percolative conduction in granular copper oxide superconductors, Phys. Rev. B 55 (1997) 1209–1215.
[11] P. Muné, E. Govea-Alcaide, R.F. Jardim, Influence of the compacting pressure on the dependence of the critical current with magnetic field in polycrystalline $(Bi\text{-}Pb)_2Sr_2Ca_2Cu_3O_x$ superconductors, Physica C 384 (2003) 491–500.
[12] D. Marconi, C. Lung, A.V. Pop, The influence of pelletization pressure on normal and superconducting properties of (Bi, Pb): 2223 bulk system, J. Alloy. Compd. 579 (2013) 355–359.
[13] T. Hungria, J. Galy, A. Castro, Spark plasma sintering as a useful technique to the nanostructuration of piezo-ferroelectric materials, Adv. Eng. Mater. 11 (2009) 615.
[14] E. Giannini, V. Garnier, R. Gladyshevskii, R. Flukiger, Growth and characterization of $Bi_2Sr_2Ca_2Cu_3O_{10}$ and $(Bi,Pb)_2Sr_2Ca_2Cu_3O_{10-\delta}$ single crystals, Supercond. Sci. Technol. 17 (2004) 220–226.
[15] D. Pandey, A.K. Singh, P.K. Srivastava, A.P. Singh, S.S.R. Inbanathan, G. Singh, Towards the rapid synthesis of pure 2223 powders with $Bi_{2_x}Pb_xSr_2Ca_2Cu_30_y$ compositions by semi-wet methods II. Optimization of Pb content using Pb-Sr-Ca carbonate precursors, Physica C. 241 (1995) 279.
[16] I. García-Fornaris, I. Calzada, E. Govea-Alcaide, I.F. Machado, R.F. Jardim, Spark plasma sintering of $Bi_{1.65}Pb_{0.35}Sr_2Ca_2Cu_3O_{10+\delta}$ superconducting samples: evaluation of microstructure and mechanical properties, J. Supercond. Nov. Magn. 28 (2015) 3487.
[17] J.L. MacManusDriscoll, J.C. PinChin Wang, Bravman, R.B. Beyers, Phase equilibria and melt processing of $Bi_2Sr_2Ca_1Cu_2O_{8+x}$ tapes at reduced oxygen partial pressures, Appl. Phys. Lett. 65 (1994) 2872–2874.
[18] S.A. Salem, Studies on sintering effect on the structural and transport properties of (2223) phase, Physica C 444 (2006) 40.
[19] S. Grasso, A. Perin, R. Flükiger, Deformation-induced texture in cold-rolled Ag sheathed bi(2223) tapes, Physica C 250 (1995) 43.
[20] L. Krusin-Elbaum, A.P. Malozemoff, D.C. Cronemeyer, F. Holtzberg, J.R. Clem, H. Zhidong, New mechanisms for irreversibility in high-Tc superconductors, J. Appl. Phys. 67 (1990) 4670–4675.
[21] J.R. Clem, H. Zhidong, Theory for the hysteretic properties of the low-field dc magnetization in type-II superconductors, Phys. Rev. B 48 (1993) 13774.
[22] M.I. Petrov, I.L. Belozerova, K.A. Shaikhutdinov, D.A. Balaev, A.A. Dubrovskii, S. I. Popkov, A.D. Vasilev, O.N. Martyanov, Preparation, microstructure, magnetic and transport properties of bulk textured $Bi_{1.8}Pb_{0.3}Sr_{1.9}Ca_2Cu_3O_x$ and $Bi_{1.8}Pb_{0.3}Sr_{1.9}Ca_2Cu_3O_x$+Ag ceramics, Supercond. Sci. Technol. 21 (2008) 105019.
[23] E. Govea-Alcaide, I.F. Machado, R.F. Jardim, 10 to 25-fold increase in the transport superconducting critical current density of spark-plasma sintered Bi-2223 superconductors, J. Appl. Phys. 117 (2015) 043903.
[24] D.X. Chen, R.W. Cross, A. Sanchez, Effects of critical current density, equilibrium magnetization and surface barrier on magnetization of high temperature superconductors, Cryogenics 33 (1993) 695–703.
[25] A. Umezawa, G.W. Crabtree, J.Z. Liu, H.W. Weber, W.K. Kwok, L.H. Nunez, T. J. Moran, C.H. Sowers, Enhanced critical magnetization currents due to fast neutron irradiation in single-crystal $YBa_2Cu_3O_{7-\delta}$, Phys. Rev. B 36 (1987) 7151.
[26] F. Pérez, X. Obradors, J. Fontcuberta, X. Bozec, A. Fert, Magnetic flux penetration and creep in a ceramic $(Y,Sm)Ba_2Cu_3O_7$ superconductor, Supercond. Sci. Technol. 9 (1996) 161–175.
[27] K.H. Müller, AC susceptibility of high temperature superconductors in a critical state model, Physica C 159 (1989) 717–726.
[28] M. Weigand, M. Eisterer, E. Giannini, H.W. Weber, Mixed state properties of $Bi_2Sr_2Ca_2Cu_3O_{10+\delta}$ single crystals before and after neutron irradiation, Phys. Rev. B 81 (2010) 014516.
[29] M.R. Cimberle, C. Ferdeghini, G. Grasso, C. Rizzuto, A.S. Siri, R. Flukiger, F. Marti, Determination of the intragrain critical current density of the Bi (2223) phase inside Ag-sheathed tapes, Supercond. Sci. Technol. 11 (1998) 837–842.
[30] T. Fujii, T. Watanabe, A. Matsuda, Comparative study of transport properties of $Bi_2Sr_2Ca_2Cu_3O_{10+\delta}$ and $Bi_2Sr_2CaCu_2O_{8+\delta}$ single crystals, Physica C 357–360 (2001) 173–176.